Available online at www.sciencedirect.com
ScienceDirect
Trans. Nonferrous Met. Soc. China 31(2021) 2442−2453
Transactions of Nonferrous Metals Society of China
www.tnmsc.cn

Achieving remarkable piezoelectric activity in Sb−Mn co-modified $CaBi_4Ti_4O_{15}$ piezoelectric ceramics

Yang LIU[1], Yang YU[1], Chen-yi YIN[1], Liang ZHENG[1], Peng ZHENG[1], Wang-feng BAI[2], Li-li LI[1], Fei WEN[1], Yang ZHANG[1]

1. Lab for Nanoelectronics and Nanoelectronic Devices, Department of Electronics Science and Technology, Hangzhou Dianzi University, Hangzhou 310018, China;
2. College of Materials and Environmental Engineering, Hangzhou Dianzi University, Hangzhou 310018, China

Received 21 August 2021; accepted 6 April 2021

Abstract: $CaBi_4Ti_4O_{15}$ (CBT)-based Aurivillius high-temperature piezoceramics with different Sb−Mn co-doping amounts were synthesized via the conventional sintering technique. The influences of doping amount on the product were studied via their crystal structure, microstructure, and piezoelectric performance. It is found that an appropriate Sb−Mn co-doping amount can effectively optimize the crystal structure and decrease the oxygen vacancy concentration in CBT ceramics, leading to enhanced electrical properties. Optimized electrical performance with a high Curie temperature (T_C) of 792 °C and a remarkable piezoelectric coefficient (d_{33}) of 25 pC/N were achieved at a doping amount (x) of 0.05. Furthermore, this ceramic is found to exhibit an excellent thermal stability, with d_{33} retaining 88% of its original value after annealing at 600 °C for 2 h. Moreover, this ceramic shows a high electrical resistivity (ρ) of 1.35×10^8 Ω·cm with a small dielectric loss ($\tan\delta$) of 1.7% at 400 °C. Because of such outstanding piezoelectric performance, it is believed that these Sb−Mn co-doped CBT ceramics could be potential candidates for high-temperature piezoelectric applications.

Key words: $CaBi_4Ti_4O_{15}$; piezoelectric ceramics; piezoelectric activity; resistivity; thermal stability

1 Introduction

In recent years, numerous industries have realized improved performances for piezoelectric sensors with high operating temperatures, particularly the fields of nuclear power and gas turbine [1−3]. Aurivillius ferroelectrics with a bismuth layer structure have been extensively investigated because of their ultrahigh ferroelectric phase transition temperature and excellent thermal stability [4]. However, their reduced piezoelectric activity dramatically restrict their practical applications. Therefore, improving the piezoelectric performance of Aurivillius ferroelectrics is urgently needed.

The structure of Aurivillius ferroelectrics consists of the regular symbiosis of $(Bi_2O_2)^{2+}$ layers and pseudo-perovskite layers, which can be described as $(Bi_2O_2)^{2+}(A_{m-1}B_mO_{3m+1})^{2-}$. Here, A corresponds to a mono-, di-, or trivalent ion, B corresponds to a tetravalent, pentavalent, or hexavalent transition element, and m represents the number of octahedral layers [5, 6]. Among various Aurivillius ferroelectrics, $CaBi_4Ti_4O_{15}$ (CBT) has been widely studied, because its high Curie temperature (T_C) of 790 °C makes it attractive for high-temperature applications [7]. However, similar to other Aurivillius ferroelectric ceramics, the piezoelectric activity of pure CBT ceramics fabricated via the conventional sintering approach is generally low. Because spontaneous polarization

Corresponding author: Liang ZHENG, Tel: +86-13175112391, E-mail: zhlbsbx@hdu.edu.cn; Peng ZHENG, E-mail: zhengpeng@hdu.edu.cn
DOI: 10.1016/S1003-6326(21)65665-0

switching occurs mainly in the $a-b$ plane [8−10]. In addition, the high electrical conductivity caused by the high oxygen vacancy concentration is also a significant obstacle to their practical applications.

Recently, the mixed-valence cations co-doping strategy at the B site has been proposed to improve the piezoelectric performance of several Aurivillius ferroelectric ceramics. For instance, LI et al [11,12] prepared Cu−Nb and Cu−Ta co-doped $Bi_4Ti_3O_{12}$ ceramics. These ceramics presented outstanding piezoelectric coefficient (d_{33}) values of 38 and 34 pC/N, accompanied by high T_C values of 678 and 677 °C, respectively. CHEN et al [13,14] designed W−Cr and Mo−Cr co-doped $CaBi_2Nb_2O_9$ ceramics. Improved d_{33} values of 15 pC/N and good thermal stability were achieved. All of the studies mentioned above demonstrate that the mixed-valence cations co-doping strategy at the B site is an excellent method to enhance the piezoelectricity of Aurivillius ferroelectric ceramics. Notably, a high piezoelectric activity accompanied by an undeteriorated T_C value has also been reported in Nb−Mn and Nb−Mg co-doped CBT ceramics. This work further suggests that the mixed-valence cations co-doping strategy at the B site is also a feasible way to improve the piezoelectric properties of the CBT ceramics [6,15]. Nevertheless, this method of mixed-valence cations co-doping has rarely been applied to CBT-based ceramics, and the potential improvement mechanism has remained unclear.

In this study, CBT ceramics co-doped with mixed-valence Sb−Mn cations at the Ti site were prepared with different doping amounts. The influence of different doping amounts on the structure and electrical performance was thoroughly investigated. A remarkable piezoelectric coefficient and good thermal stability were achieved at a doping amount (x) of 0.05. Furthermore, an enhanced electrical resistivity and almost unaffected Curie temperature were obtained in this ceramic. The relevant mechanisms for the optimized piezoelectricity performance and resistivity were also systematically discussed.

2 Experimental

$CaBi_4Ti_{4-x}(Sb_{2/3}Mn_{1/3})_xO_{15}$ (CBTSM-x) ceramics (x=0, 0.02, 0.04, 0.05, 0.06, and 0.1) were synthesized via the conventional sintering technique. TiO_2 (99.8%), $CaCO_3$ (99.99%), Bi_2O_3 (99.99%), and $MnCO_3$ (99.95%) were employed as raw materials. Sb_2O_3 (99.5%) was selected as the Sb source, and it is oxidized to Sb_2O_5 at high temperature [16]. The raw materials were mixed using a planetary ball mill with ethyl alcohol. Calcination was carried out at 825 °C for 4 h. The powders were then ball milled again for 12 h. Finally, these powders were mixed with polyvinyl alcohol (PVA) and pressed into discs under a pressure of 150 MPa. After removing PVA, the discs were sintered in the temperature range of 1000−1100 °C for 1 h.

The surface morphology of the ceramics was investigated using scanning electron microscopy (SEM, JEOL JSM6460-LV). The Archimedes drainage method was used for density measurements. The crystalline phases of the ceramic powders were determined via X-ray diffraction (XRD, Ultima IV). The Raman spectra were measured using a Raman spectrometer (iHR320). The dielectric performance was measured with an impedance analyzer (Keysight E4990A). The DC conduction was measured using a high-resistance meter (Keithley 2410) under a voltage of 10 V. An impedance analyzer (Keysight E4990A) was employed to measure the AC conduction in the frequency range between 100 Hz and 10 MHz. For the piezoelectric characterization, a poling treatment of the obtained ceramics was carried out under a 14−16 kV/cm electric field at 160 °C for half an hour. Subsequently, the piezoelectric constants (d_{33}) were recorded at room temperature with a piezo-d_{33} meter (ZJ-3AN). The ferroelectric properties were measured using a ferroelectric analyzer (RADIANT Technologies Inc RT1-Premier II).

3 Results and discussion

3.1 Microstructure and phase structure characterization

Figure 1(a) shows the XRD patterns of the CBTSM-x ceramics obtained in the 2θ range from 20° to 60°. All of the ceramics exhibit a pure Aurivillius phase structure, and no other impurities can be observed according to the standard PDF card (No. 52−1640). This indicates that the co-doped

ions were successfully incorporated into the CBT lattice. The highest intensity peak was found to correspond to the (119) reflection plane, which is consistent with the most intense reflections (112m+1) typical of Aurivillius ferroelectrics [17]. An additional peak can be seen on the left of the (119) peak, and its intensity increased as the doping amount increased. This peak is consistent with the $Bi_{1.74}Ti_2O_{6.624}$ impurity phase, according to the standard PDF card (No. 89−4732). Normally, $Bi_2Ti_2O_7$ can be easily formed at the early stages of the thermal process because of its excellent relative stability in the Bi_2O_3−TiO_2 system [18,19]. When the ambient temperature exceeded over 700 °C, the $Bi_2Ti_2O_7$ phase began to change into the $CaBi_4Ti_4O_{15}$ phase. However, because of the volatilization of Bi ions, a certain amount of $Bi_2Ti_2O_7$ probably converted into $Bi_{1.74}Ti_2O_{6.624}$, as its Bi/Ti ratio was lower than that of $CaBi_4Ti_4O_{15}$, resulting in a structural cross-over. The zoomed-in view of the (117) and (119) diffraction peaks are illustrated in Figs. 1(b) and 1(c). Both two peaks shift to higher 2θ degrees when the doping amount increases from 0 to 0.04. They further shift to lower degree with higher doping amount to 0.1. To further determine the variation of the crystal structure, the lattice parameter dependence on different doping amounts is illustrated in Fig. 2(a). The a and b values decrease as x increases from 0 to 0.05, whereas the c value increases, giving rise to an overall decreasing cell volume V. However, for x>0.05, the a and b values increase, whereas the c value decreases slightly, causing V to increase. The increasing V in the high-doping region might be caused by the larger effective ionic radius of ($Sb^{5+}_{2/3}Mn^{2+}_{1/3}$) (0.623 Å) compared to that of Ti^{4+}(~0.605 Å). On the other hand, the lattice shrinkage in the low-doping region might be ascribed to the variation of electronegativity of the doped elements. As revealed by Pauling, Sb has a

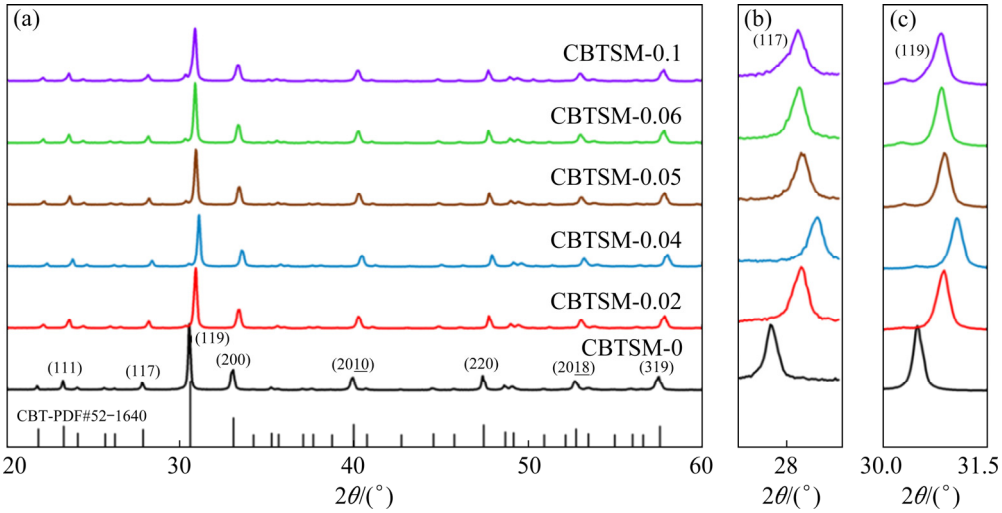

Fig. 1 XRD patterns of CBTSM-x ceramics (a), enlarged view of (117) (b) and (119) (c) diffraction peaks

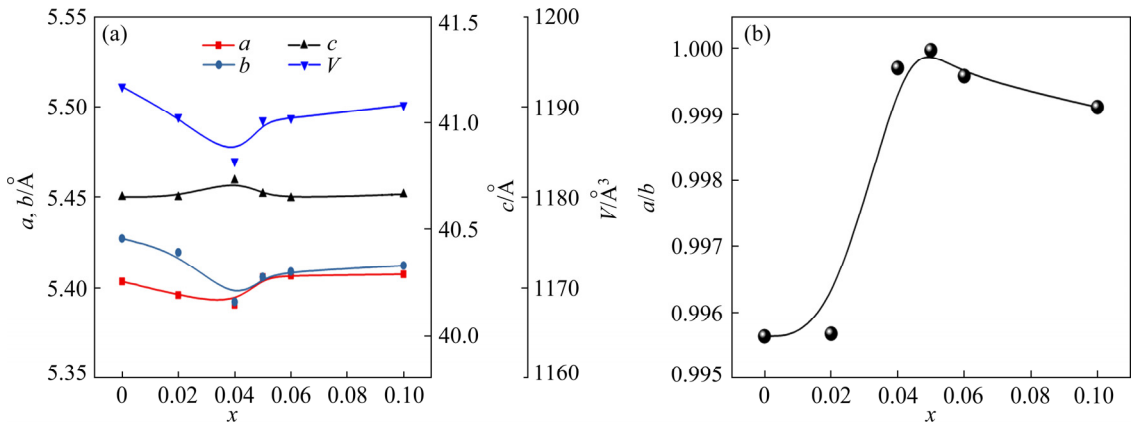

Fig. 2 Lattice parameters a, b, c and unit cell V as function of x (a), and a/b ratio (b) of CBTSM-x ceramics as function of x

larger electronegativity (2.05) than Ti (1.54). This could lead to a larger interaction between Sb and O, thus shortening the Sb—O bond in the octahedron, which may explain the lattice shrinkage at x<0.05 [20]. In addition, the Mn^{2+} ion might be partially oxidized to the Mn^{4+} ion in the low-doping region [21,22], giving rise to a smaller effective ionic radius for $Sb^{5+}_{2/3}Mn^{4+}_{1/3}$ (0.577 Å) compared to that of Ti^{4+}. To assess the degree of lattice distortion, Fig. 2(b) shows the a/b ratio dependence as a function of x. The value of the a/b ratio first increased and then fell upon increasing the doping amount, reaching a maximum value at x=0.05. The result demonstrates that the tetragonality of the CBT lattice improved, whereas the anisotropy decreased with Sb−Mn co-doping. This finding may facilitate the switching of the spontaneous polarization in the $a-b$ plane and yield a superior piezoelectric performance [23].

Figure 3(a) shows the Raman spectra of the CBTSM-x samples recorded at room temperature. Several sharp peaks at ~125, ~156, ~270, ~555, and ~860 cm^{-1} are in agreement with the previous works [24,25]. The mode at ~125 cm^{-1} can be attributed to the vibration of the Bi^{3+} ion in the $(Bi_2O_2)^{2+}$ structure [26]. On the other hand, the vibrations of the A-site ions in the pseudo-perovskite layer are related to the mode at ~156 cm^{-1} [27]. The modes at ~270 cm^{-1} (B_{2g} and B_{3g} modes) can be assigned to the O—Ti—O vibration [28]. In comparison, the Raman peak at ~555 cm^{-1} (A_{1g} mode) corresponds to the relative displacement of the oxygen atom in the TiO_6 octahedron, and the mode at 839 cm^{-1} (B_{1g} mode) is associated with the stretching of the TiO_6 octahedron [24]. No extra peaks are observed, which further demonstrates that the co-doped Sb and Mn have been properly incorporated into the CBT lattice. Moreover, enlarged Raman peaks in various frequency regions are presented in Figs. 3(b)−(f). No clear shift can be detected in the phonon modes, which may be attributed to the

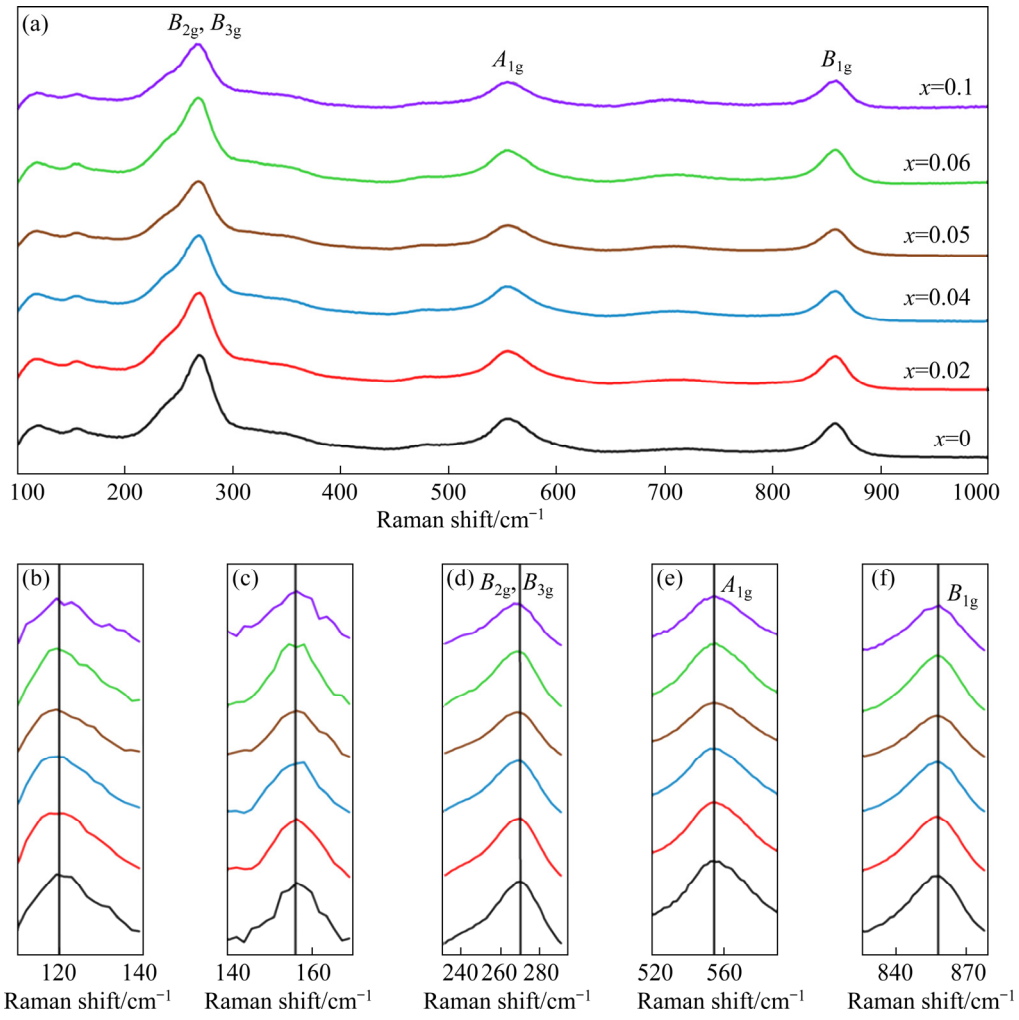

Fig. 3 Raman spectra of CBTSM-x ceramics (a), and Raman peaks in various frequency regions (b−f)

small co-doping amount of Sb and Mn.

The microstructures of the natural surface of the obtained CBTSM-x ceramics are shown in Fig. 4. As illustrated, all of the samples show similar microstructures with strongly anisotropic grains, which is a typical characteristic of the Aurivillius ceramics [28]. However, microstructures with a higher relative density (ρ_0) are observed with increased doping concentration. This behavior might be attributed to the addition of Mn, which enhances the sinterability of the ceramic by promoting the diffusion of grain boundaries [29]. Figure 5 displays the elemental mappings of the CBTSM-0.05 sample. It can be seen that each element shows a uniform distribution in the sample, further confirming the diffusion of Sb and Mn into the CBT lattice.

3.2 Dielectric behavior

Figure 6(a) presents the dependence of dielectric permittivity (ε_r) of the Sb−Mn co-doped CBT ceramics on temperature at 1 MHz. The dielectric permittivity of all of the ceramics increases slowly as the temperature increases to 500 °C, and then it increases sharply, with a unique transition temperature at ~790 °C. The T_C value corresponding to x is shown in Fig. 6(b). The T_C values are extremely close for all of the ceramics, lying in the range of 792−793 °C. Figure 6(c) illustrates the temperature dependence of the dielectric loss (tan δ) for all of the samples. The values of tan δ are relatively low for temperatures below 450 °C but rise sharply when the temperature is further increased. To illustrate the changes in tan δ induced by Sb−Mn co-doping, the tan δ values

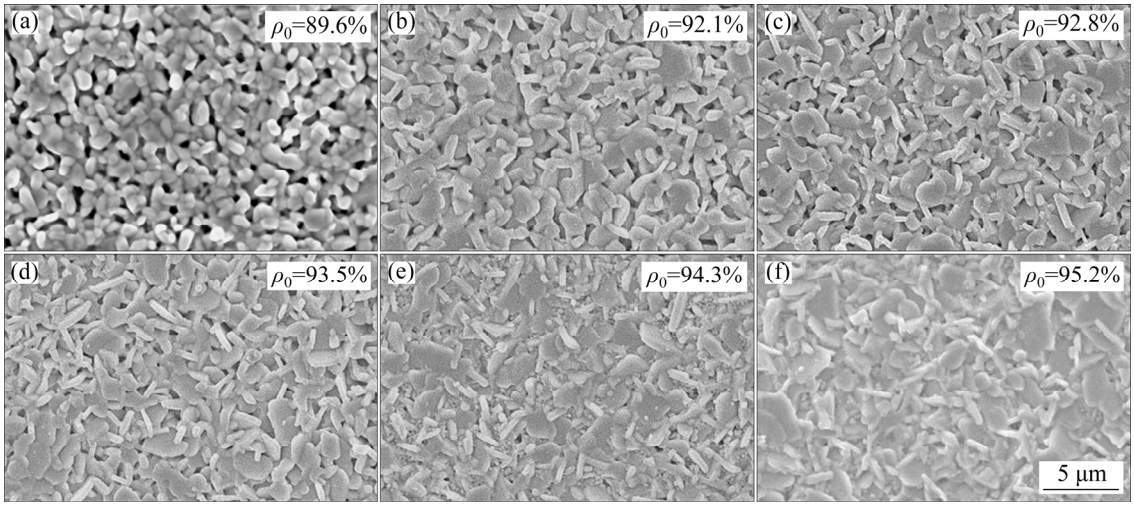

Fig. 4 SEM images collected on natural surface of ceramics: (a) CBTSM-0; (b) CBTSM-0.02; (c) CBTSM-0.04; (d) CBTSM-0.05; (e) CBTSM-0.06; (f) CBTSM-0.1

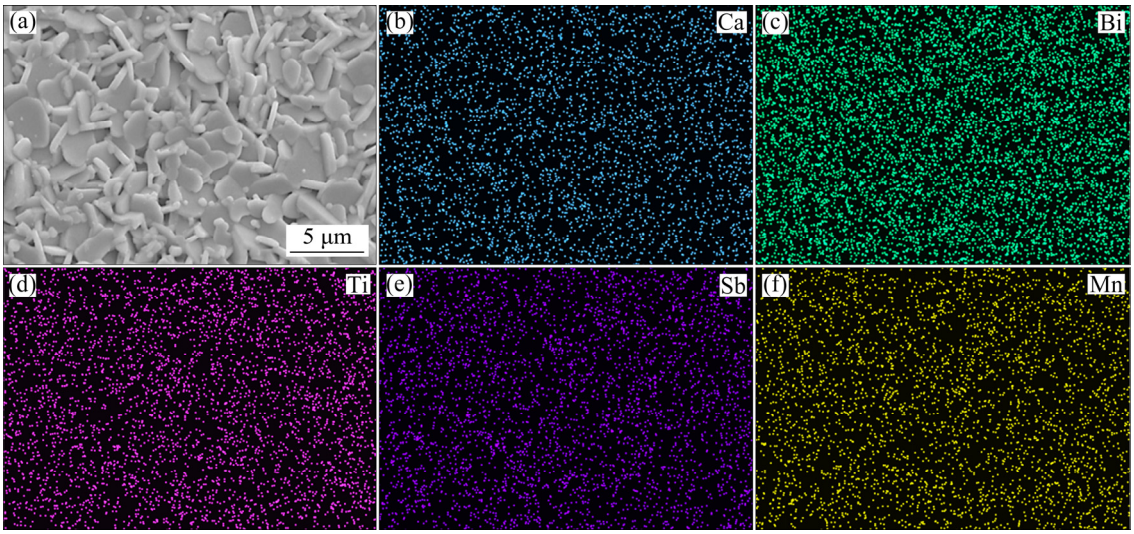

Fig. 5 Elemental mappings of CBTSM-0.05 ceramic

obtained at 400 °C for all of the ceramics are presented in Fig. 6(d). The tanδ values first decreases and then increases upon increasing doping amount. The CBTSM-0.05 ceramic exhibits a much lower tan δ value (1.7%) than the CBTSM-0 ceramic (2.9%), which may be caused by a decrease in the oxygen vacancy concentration after co-doping [30−33]. These outstanding dielectric properties will facilitate the practical application of this ceramic in high-temperature fields.

3.3 Piezoelectric and ferroelectric properties

Figure 7(a) shows the piezoelectric constant (d_{33}) of CBT ceramics with different Sb−Mn co-

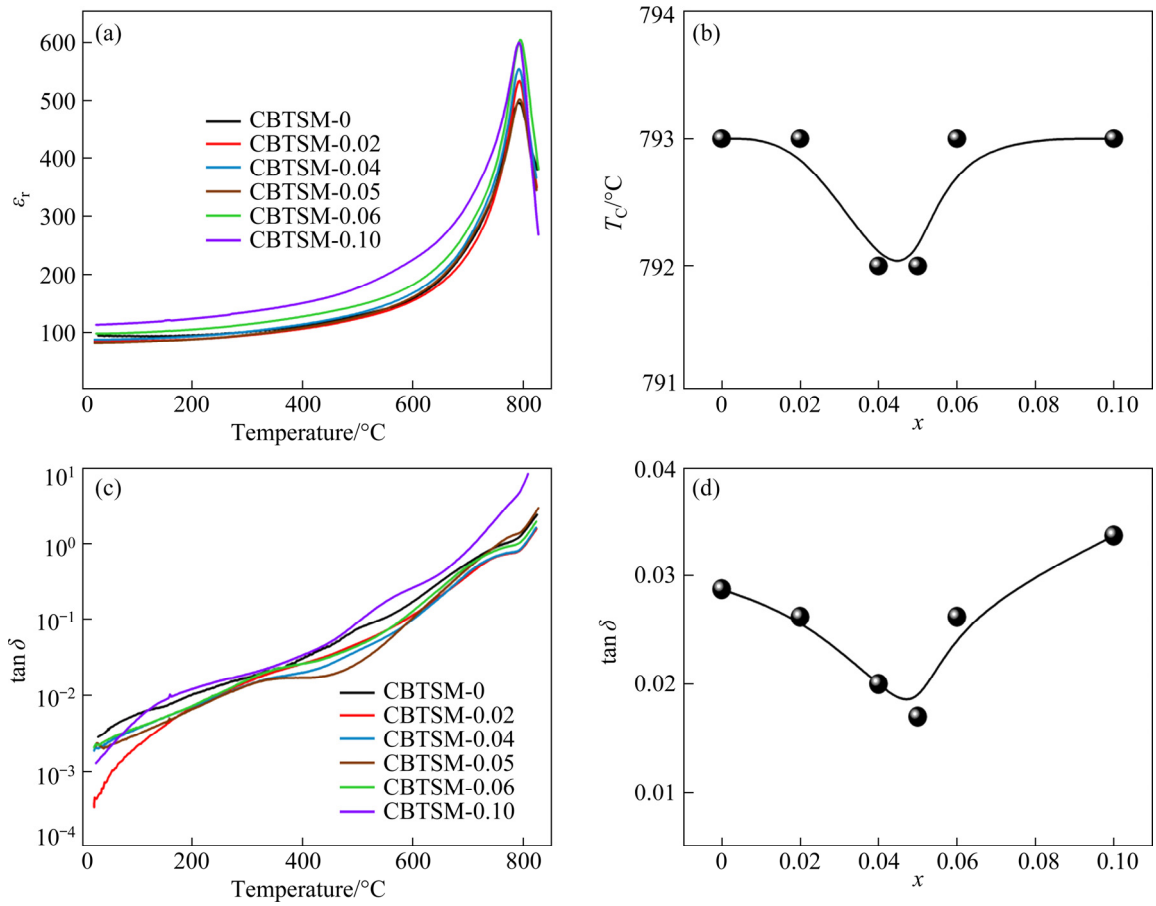

Fig. 6 Dependence of ε_r on temperature for CBTSM-x ceramics at 1 MHz (a), correlation between T_C and x (b), tan δ values at 1 MHz for CBTSM-x ceramics as function of temperature (c), and tan δ values obtained at 400 °C as function of x (d)

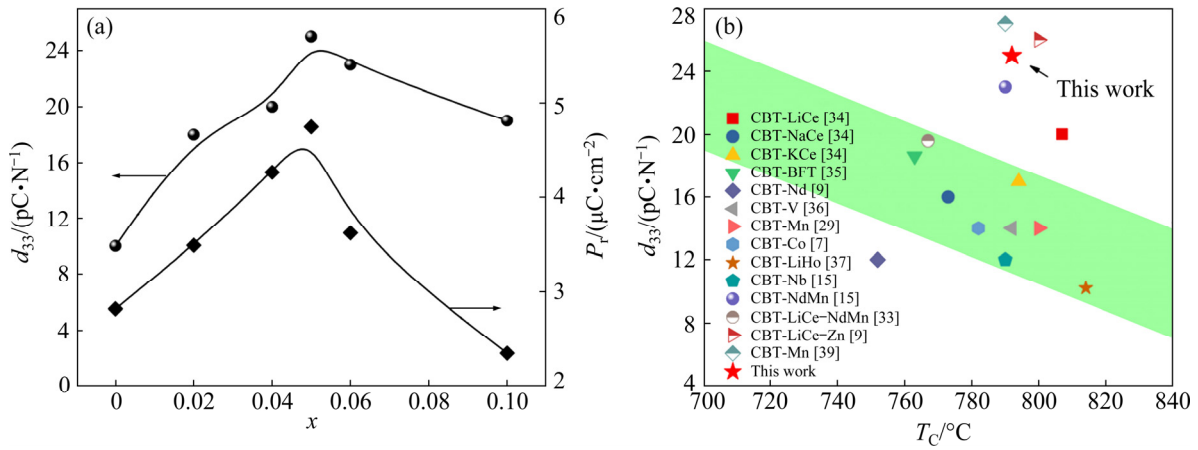

Fig. 7 Dependence of piezoelectric coefficient (d_{33}) and remnant polarization (P_r) on doping amount (a), and comparison between T_C and d_{33} values measured and those reported in previous works (b)

doping amounts. The d_{33} value first increases and then declines with increased Sb−Mn content, showing the highest value of 25 pC/N at x=0.05. All of the co-doped CBTSM-x ceramics have a larger d_{33} value than the pure CBT ceramic, illustrating that co-doping with Sb−Mn efficiently enhances the piezoelectricity of the CBT ceramic. To provide a better evaluation of the piezoelectric properties exhibited by the sample at x=0.05, a comparison between the T_C and d_{33} values measured here and the values reported in the literature is shown in Fig. 7(b) [7,9,15,29,33−39]. Most of the previous research results are located in the green region, while the CBTSM-0.05 sample clearly stands out because of its excellent piezoelectricity and high T_C.

It is thought that the piezoelectric properties often depend on ferroelectricity. The P−E loops and I−E curves of CBTSM-x ceramics measured at 10 Hz and 100 °C under an electric field of 180 kV/cm are presented in Figs. 8(a) and (b), respectively. All of the ceramics show saturated hysteresis loops with significant ferroelectric switching peaks. The remnant polarization (P_r) values are illustrated in Fig. 7(a). The P_r value first increases and then decreases with increased doping amount, reaching a maximum value at x = 0.05. The enhanced ferroelectricity may be ascribed to the improvement of the tetragonal structure [11]. It is worth noting that the variation trend of the P_r value is similar to that of the d_{33} value, suggesting that the large piezoelectric activity may be partly attributed to the enhanced P_r.

3.4 Resistivity and complex impedance

Resistivity is also a key indicator for evaluating the electrical properties of Aurivillius ferroelectric ceramics. Figure 9(a) displays the variation of the electrical resistivity with respect to temperature for the Sb−Mn co-doped CBT ceramics. The electrical resistivity ρ decreased with

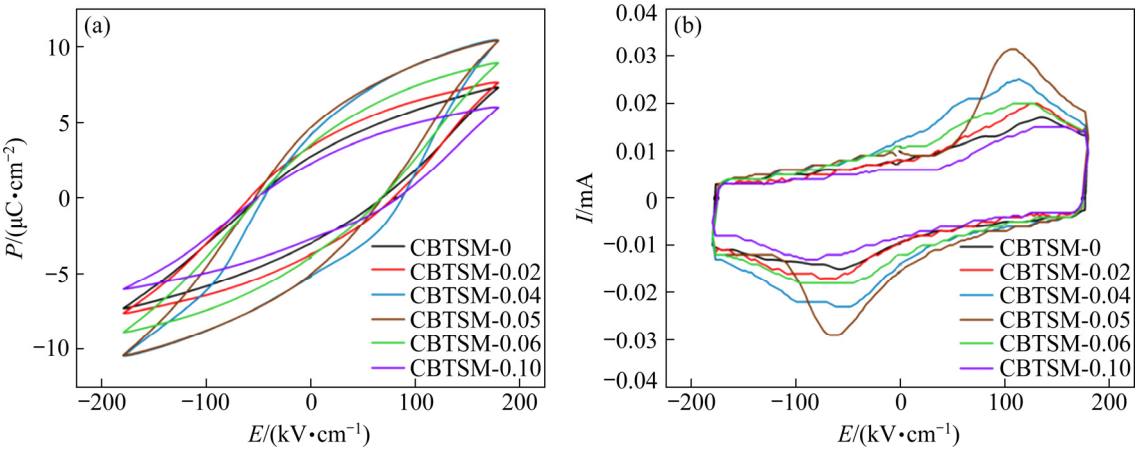

Fig. 8 P–E loops (a) and I–E (b) curves for CBTSM-x ceramics

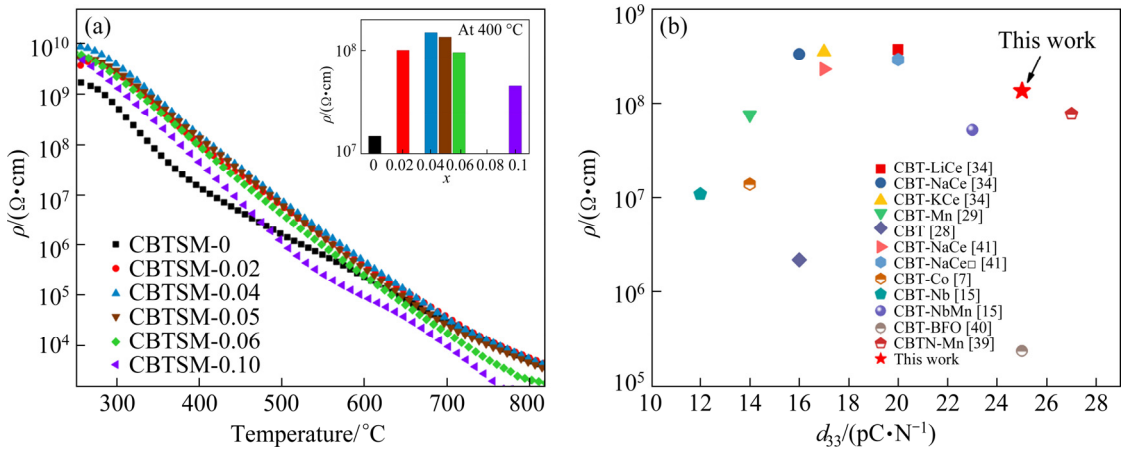

Fig. 9 Variation of ρ as function of temperature for Sb−Mn co-doped CBT ceramics (The inset illustrates the correlation between ρ and x at 400 °C) (a), and comparison between d_{33} and ρ values measured at 400 °C and those of previous works (b)

increasing temperature for all of the ceramics, indicating that the carriers are thermally activated. The resistivity measured at 400 °C first increases and then decreases as the Sb−Mn co-doping amount increases, as displayed in the inset of Fig. 9(a). The CBTSM-0.05 sample exhibits a ρ of 1.35×10^8 Ω·cm, which is an order of magnitude higher than that of the undoped ceramic (1.48×10^7 Ω·cm). It is worth noting that the CBTSM-0.05 ceramic simultaneously exhibits a significant resistivity and a remarkable d_{33} value compared with the CBT-based ceramics investigated in previous reports [7,15,28,29,34,39−41], suggesting that Sb−Mn co-doping can comprehensively boost the electrical properties of the CBT ceramic.

To investigate the possible mechanisms behind the enhanced electrical resistivity, the complex impedances of the CBTSM-0 and CBTSM-0.05 ceramics were measured from 100 Hz to 10 MHz at different temperatures, and the results are shown in Figs. 10(a, b), respectively. Only one semicircle can be detected, indicating that grains play a dominant role in the conductivity of the ceramics [42]. An equivalent circuit model (R-CPE-C), shown in the inset of Fig. 10(a), was adopted to fit the complex impedances with the aid of Z-view software. Good fittings to the experimental data were achieved for both ceramics. The CPE-P values of the constant phase element (CPE) lie between 0.46 and 0.54, which may be attributed to the Warburg diffusion related to the oxygen migration process. The diameter of the semicircle decreases with increasing temperature, indicating a reduction in resistance. The activation energy (E_a) can be calculated using the Arrhenius law:

$$\sigma=A\exp[E_a/(kT)] \quad (1)$$

where σ corresponds to the conductivity, A represents the pre-exponent factor, k is the Boltzmann constant, and T is the temperature. Figure 11(a) shows the relationship between conductivity and temperature for the CBTSM-x ceramics. The obtained E_a values are presented in Fig. 11(b). As seen, the calculated E_a value for the pristine CBT ceramic is 1.25 eV, indicating that the conduction is dominated by the migration of oxygen vacancies in the grains [13,33]. However, higher E_a values of 1.43−1.67 eV were acquired for the Sb−Mn co-doped ceramics, indicating intrinsic charge carrier conduction [43]. The higher E_a values suggest that the oxygen vacancy concentration is significantly reduced because of Sb−Mn co-doping.

To obtain deeper insight into the reduced oxygen vacancy concentration, a detailed electrochemical analysis is provided here. During the sintering process, Bi_2O_3 volatilization is unavoidable, and oxygen vacancies ($V_o^{\bullet\bullet}$) are generated to maintain the electric neutrality (Eq. (2)) [11]. Evidently, the Sb_2O_5 donor dopant can directly reduce the oxygen vacancy concentration (Eq. (3)), which is beneficial for the improvement of the electrical resistivity. In contrast, the acceptor substitution of Mn^{2+} for Ti^{4+} generates lattice defects (Mn''_{Ti}) and oxygen vacancies, as expressed by Eq. (4) [31]. Generally, the extra oxygen vacancies should cause a reduction in the resistivity. However, opposite results have been obtained for the W−Mn and Sb−Cu doped BIT ceramics [22,31]. It was speculated that the movement of these extra oxygen vacancies is limited near defect centers (Mn''_{Ti}) because of the formation of strongly combined defect dipoles ($Mn''_{Ti}-V_{oe}^{\bullet\bullet}$), which do not contribute to the

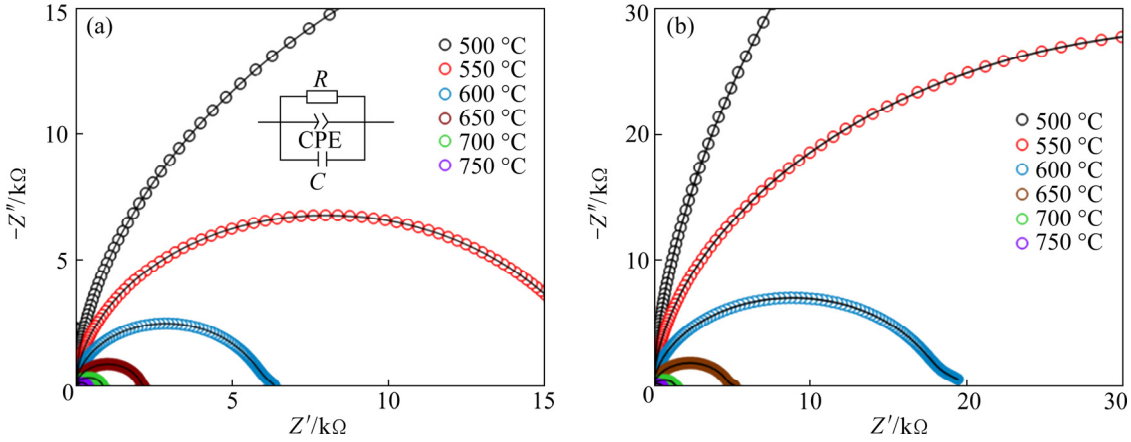

Fig. 10 Nyquist diagrams for CBTSM-0 (a) and CBTSM-0.05 (b) at 500−750 °C

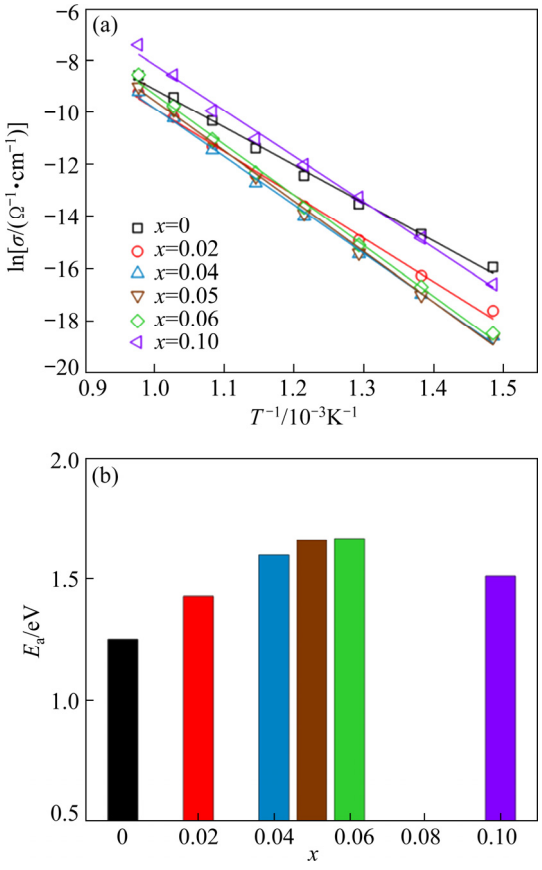

Fig. 11 Correlation between $\ln\sigma$ and T^{-1} for various doping amounts (a), and variation trends of E_a with various x (b)

conductive process of the ceramic, as described by Eq. (5) [31]. On the contrary, the number of intrinsic oxygen vacancies decreases to retain the overall balance for the oxygen vacancy amount. In addition, the Mn^{2+} ions in the raw oxides are partially oxidized to the Mn^{4+} ions in the low-doping region. The Mn^{4+} ions production might represent another reason for the reduction of the oxygen vacancies in the low-doping region [44, 45], which can be expressed by Eq. (6). Generally speaking, the reduced oxygen vacancy concentration in the Sb−Mn co-doped CBT ceramics might be ascribed to the combined action of the Sb donor doping and Mn acceptor doping.

$$Bi_2O_3 \rightarrow 2Bi(g)\uparrow + 3/2O_2(g)\uparrow + 2V_{Bi}''' + 3V_o^{\cdot\cdot} \quad (2)$$

$$Sb_2O_5 + V_o^{\cdot\cdot} \xrightarrow{2TiO_2} 2Sb_{Ti}^{\cdot} + 5O_o^{\times} \quad (3)$$

$$MnCO_3 \xrightarrow{TiO_2} Mn_{Ti}'' + V_{oe}^{\cdot\cdot} + O_o^{\times} + CO_2(g)\uparrow \quad (4)$$

$$Mn_{Ti}'' + V_{oe}^{\cdot\cdot} \rightarrow (Mn_{Ti}'' - V_{oe}^{\cdot\cdot}) \quad (5)$$

$$Mn^{2+} + V_o^{\cdot\cdot} + 0.5O_2 \rightarrow Mn^{4+} + O_o^{\times} \quad (6)$$

3.5 Thermal stability

The thermal stability of the Aurivillius piezoelectric materials is an important indicator of their practical applications. To illustrate the thermal stability of CBTSM-x ceramics, thermal annealing behaviors at different temperatures are presented in Fig. 12(a). The poled samples were annealed from 25 to 800 °C in steps of 50 °C for 2 h. Subsequently, the d_{33} values were measured at room temperature. The piezoelectric performance remains stable up to 500 °C. However, when the annealing temperature exceedes over 500 °C, the d_{33} value for all of the samples decreases. This may be because depolarization occurs at high temperatures, as a consequence of the space charge movement [22]. Despite this, the d_{33} value of the CBTSM-0.05 ceramic retains 88% of the starting value after being annealed for 2 h at 600 °C. Figure 12(b) illustrates a comparison between the thermal annealing behavior of the CBTSM-0.05 ceramic measured in this work and those reported in the Refs. [7,15,33,37,40,46,47].

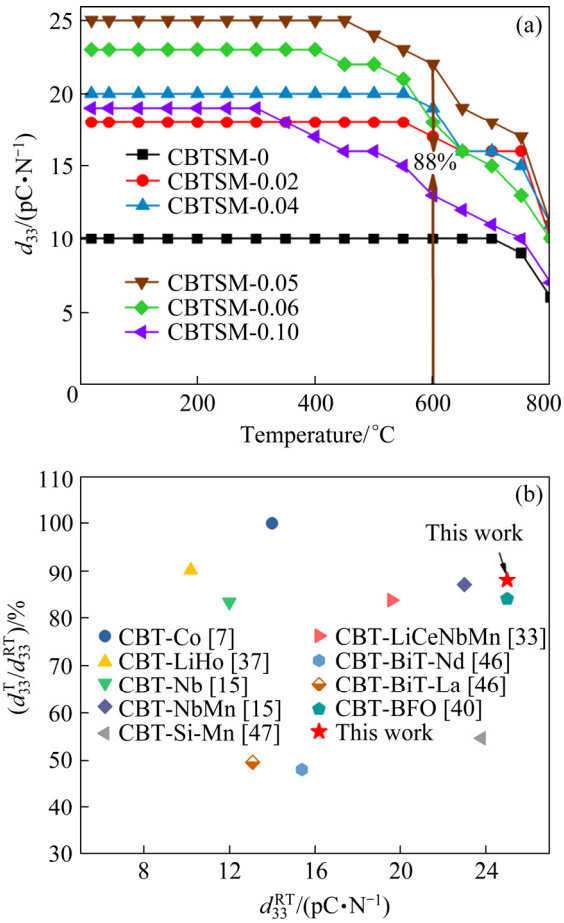

Fig. 12 Thermal depolarization behavior of CBTSM-x ceramics (a), and comparison between thermal stability behavior at 600 °C reported in present work and existing literature (b)

Compared with other works, the CBTSM-0.05 ceramic shows an excellent thermal stability with remarkable piezoelectric activity. A reduced number of defects may be an important underlying reason for this behavior. Also, the thermal stability of piezoelectric ceramics is considered to depend significantly on domain wall motion. In this work, as the tetragonality of the lattice structure was optimized via Sb−Mn co-doping, the number of unstable non-180° domain walls should be reduced, which might account for the excellent thermal stability [48].

4 Conclusions

(1) Ti-site Sb−Mn co-doped $CaBi_4Ti_{4-x}(Sb_{2/3}Mn_{1/3})_xO_{15}$ ceramics were synthesized via the conventional sintering method.

(2) Addition of Sb and Mn resulted in an efficient enhancement of the tetragonal distortion and in a reduction of the oxygen vacancy amount, thus promoting optimized piezoelectric activity and superior electrical resistivity.

(3) The CBTSM-0.05 ceramic exhibits the best electrical properties with a greatly enhanced piezoelectric activity (d_{33}=25 pC/N). It also presents outstanding thermal stability with the d_{33} value retaining 88% of its original value after annealing at 600 °C for 2 h.

(4) The CBTSM-0.05 ceramic also exhibits improved resistivity (1.35×10^8 Ω·cm at 400 °C) and a high T_C (792 °C).

(5) The Sb−Mn co-doping method can be an effective approach to improve the electrical properties of CBT-based ceramics.

Acknowledgments

The authors are grateful for the financial support from the Key Research and Development Project of Zhejiang Province, China (No. 2017C01056).

References

[1] TURNER R C, FUIERER P A, NEWNHAM R E, SHROUT T R. Materials for high temperature acoustic and vibration sensors: A review [J]. Applied Acoustics, 1995, 41: 299−324.

[2] MOHAMMADI AREF S, GHAFOURI M. Electrophysical properties of ceramic−polymer composite films as function of sintering temperature [J]. Transactions of Nonferrous Metals Society of China, 2018, 28: 495−501.

[3] CHENG Hua-bei, XIAO Jian, GAO Peng, YAN Yun-yun, GAO Shuan-ping, DU Hong-liang. Sol−gel auto-combustion synthesis of $K_xNa_{1-x}NbO_3$ nanopowders and ceramics: Dielectric and piezoelectric properties [J]. Transactions of Nonferrous Metals Society of China, 2018, 28: 1801−1807.

[4] ZHANG Shu-ju, YU Fa-peng. Piezoelectric materials for high temperature sensors [J]. Journal of the American Ceramic Society, 2011, 94: 3153−3170.

[5] XING Xing-he, CAO Feng, PENG Zhi-hang, XIANG Yang. Electrical properties and sintering characteristics of zirconium doped $CaBi_2Nb_2O_9$ ceramics [J]. Ceramics International, 2018, 44: 17326−17332.

[6] LI Li-li, YUAN Hong-bin, HUANG Pei-ming, ZHANG Yu-hao, SHENG Lin-sheng, ZHENG Peng, ZHANG Liang, WEN Fei, WU Wei, XU Zhuo. Enhanced piezoelectricity and excellent thermal stabilities in Nb−Mg co-doped $CaBi_4Ti_4O_{15}$ Aurivillius high Curie temperature ceramics [J]. Ceramics International, 2020, 46: 2178−2184.

[7] ZHAO Tian-long, WANG Chun-ming, WANG Chun-lei, WANG Yi-ming, DONG Shu-xiang. Enhanced piezoelectric properties and excellent thermal stabilities of cobalt-modified Aurivillius-type calcium bismuth titanate ($CaBi_4Ti_4O_{15}$) [J]. Materials Science and Engineering B, 2015, 201: 51−56.

[8] KORZUNOVA L. Piezoelectric ceramics for high-temperature transducers [J]. Ferroelectrics, 1992, 134: 175−180.

[9] ZENG Jiang-tao, LI Yong-xiang, WANG Dong, YIN Qing-rui. Electrical properties of neodymium doped $CaBi_4Ti_4O_{15}$ ceramics [J]. Solid State Communications, 2005, 133: 553−557.

[10] FU Bin, HOU Yang-lu, LI Ting, FU Xing-hua. Effects of Sr and Mn-doping on the electrical properties of $CaBi_4Ti_4O_{15}$-based ceramics [J]. Key Engineering Materials, 2013, 575−576: 494−498.

[11] LI Xu-dong, CHEN Zhen-ning, SHENG Lin-sheng, LI Li-li, BAI Wang-feng, WEN Fei, ZHENG Peng, WU Wei, ZHENG Liang, ZHANG Yang. Remarkable piezoelectric activity and high electrical resistivity in Cu/Nb co-doped $Bi_4Ti_3O_{12}$ high temperature piezoelectric ceramics [J]. Journal of European Ceramic Society, 2019, 39: 2050−2057.

[12] LI Xu-dong, CHEN Zhen-ning, SHENG Lin-sheng, DU Juan, BAI Wang-feng, LI Li-li, WEN Fei, ZHENG Peng, WU Wei, ZHENG Liang, ZHANG Yang. Large enhancement of piezoelectric properties and resistivity in Cu/Ta co-doped $Bi_4Ti_3O_{12}$ high temperature piezoceramics [J]. Journal of American Ceramic Society, 2019, 102: 7366−7375.

[13] CHEN Zhen-ning, ZHANG Yu-hao, HUANG Pei-ming, LI Xu-dong, DU Juan, BAI Wang-feng, LI Li-li, WEN Fei, ZHENG Peng, WU Wei, ZHENG Liang, ZHANG Yang. Enhanced piezoelectric properties and thermal stability in Mo/Cr co-doped $CaBi_2Nb_2O_9$ high-temperature piezoelectric ceramics [J]. Journal of Physics & Chemistry Solids, 2020, 136: 109195.

[14] CHEN Zhen-ning, SHENG Lin-sheng, LI Xu-dong, ZHENG Peng, BAI Wang-feng, LI Li-li, WEN Fei, WU Wei, ZHENG Liang, CUI Jia-dong. Enhanced piezoelectric properties and electrical resistivity in W/Cr co-doped $CaBi_2Nb_2O_9$ high-temperature piezoelectric ceramics [J]. Ceramics

International, 2019, 45: 6004−6011.

[15] SHEN Zong-yang, SUN Hua-jun, TANG Yan-xue, LI Yue-ming, ZHANG Shu-jun. Enhanced piezoelectric properties of Nb and Mn co-doped $CaBi_4Ti_4O_{15}$ high temperature piezoceramics [J]. Materials Research Bulletin, 2015, 63: 129−133.

[16] HOU Jun-gang, QU Yuan-fang, VAISH R, KRSMANOVIC D, KUMARZ R V. Effect of Sb substitution on the structural and electrical properties of $Bi_4Ti_{3-2x}Nb_xTa_xO_{12}$ Ceramics [J]. Journal of American Ceramic Society, 2011, 94: 2523−2529.

[17] YAN Hai-xue, ZHANG Zhen, ZHU Wei-min, HE Lian-xin, YU You-hua, LI Cheng-en, ZHOU Jia-guang. The effect of (Li,Ce) and (K,Ce) doping in Aurivillius phase material $CaBi_4Ti_4O_{15}$[J]. Materials Research Bulletin, 2004, 39: 1237−1246.

[18] NIBOU L, AFTATI A, EL FARISSI M, MERCURIO J P. Chemical fabrication $SrBi_4Ti_4O_{15}$ thin films [J]. Journal of the European Ceramic Society, 1999, 19: 1383−1386.

[19] XIAO Ping, ZHENG Qiao-ji, TIAN Mi-jie, GUO Yong-quan, WU Xiao-chun, XU Cheng-gang, LIN Dun-min. Enhanced ferroelectricity/piezoelectricity, bright blue/yellow emission and excellent thermal stability in $Ca_{1-x}(LiDy)_{x/2}Bi_4Ti_4O_{15}$ lead-free multifunctional ceramics [J]. RSC Advances, 2016, 6: 16387−16394.

[20] SHI Liang, ZHANG Bo-ping, LIAO Qing-wei, ZHU Li-feng, ZHAO Lei, ZHANG Dai-bing, GUO Dong. Piezoelectric properties of Fe_2O_3 doped $BiYbO_3$−$Pb(Zr,Ti)O_3$ high Curie temperature ceramics [J]. Ceramics International, 2014, 40: 11485−11491.

[21] TANG Yan-xue, SHEN Zong-yang, DU Qiu-xiang, ZHAO Xiang-yong, WANG Fei-fei, QIN XIAO-mei, WANG Tao, SHI Wang-zhou, SUN Da-zhi, ZHOU Zhi-yong, ZHANG Shu-jun. Enhanced pyroelectric and piezoelectric responses in W/Mn-codoped $Bi_4Ti_3O_{12}$ Aurivillius ceramics [J]. Tungsten Compounds, 2018, 38: 5348−5353.

[22] CHEN Yu, PEN Zhi-hang, WANG Qing-yuan, ZHU Jia-guo. Crystalline structure, ferroelectric properties, and electrical conduction characteristics of W/Cr co-doped $Bi_4Ti_3O_{12}$ ceramics [J]. Journal of Alloys and Compounds, 2014, 612: 120−125.

[23] SHRIVASTAVA V, JHA A K, MENDIRATTA R G. Dielectric studies of La and Pb doped $SrBi_2Nb_2O_9$ferroelectric ceramic [J]. Materials Letters, 2006, 60: 1459−1462.

[24] HE Xin-hua, WANG Bin, FU Xiao-yi, CHEN Zhi-wu. Structural, electrical and piezoelectric properties of V-, Nb- and W-substituted $CaBi_4Ti_4O_{15}$ ceramics [J]. Journal of Materials Science: Materials in Electronics, 2014, 25: 3396−3402.

[25] KOJIMA S, IMAIZUMI R, HAMAZAKI S, TAKASHIGE M. Raman scattering study of bismuth layer—Structure ferroelectrics [J]. Japanese Journal of Applied Physics, 1994, 33: 5559−5564.

[26] OSADA M, TADA M, KAKIHANA M, WATANABE T, FUNAKUBO H. Cation distribution and structural instability in $Bi_{4-x}La_xTi_3O_{12}$ [J]. Japanese Journal of Applied Physic, 2001, 40: 5572−5575.

[27] ZHU Jun, CHEN Xiao-bing, ZHANG Zeng-peng, SHEN Jian-cang. Raman and X-ray photoelectron scattering study of lanthanum-doped strontium bismuth titanate [J]. Acta Materialia, 2005, 53: 3155−3162.

[28] TANWAR A, SREENIVAS K, GUPTA V. Effect of orthorhombic distortion on dielectric and piezoelectric properties of $CaBi_4Ti_4O_{15}$ ceramics [J]. Journal of Applied Physics, 2009, 105: 084105.

[29] ZHANG Shu-jun, KIM N, SHROUT T R, KIMURA M, ANDO A. High temperature properties of manganese modified $CaBi_4Ti_4O_{15}$ ferroelectric ceramics [J]. Solid State Communications, 2006, 140: 154−158.

[30] LONG Chang-bai, FAN Hui-qing, LI Meng-meng, REN Peng-rong, CAI Yu. A candidate for lead-free ultrahigh-temperature piezoelectrics: the excellent electro-mechanical properties of Aurivillius oxides, $Ca_{1-5x}Li_{2x}Nd_{2x}\square_xBi_2Nb_{2-2x}Sc_xW_xO_{9-15x}$ [J]. CrystEngComm, 2013, 15: 10212−10221.

[31] LI Xu-dong, ZHU Ling-li, HUANG Pei-ming, CHEN Zhen-ning, BAI Wang-feng, LI Li-li, WEN Fei, ZHENG Peng, WU Wei, ZHENG Liang, ZHANG Yang. Reduction of oxygen vacancy concentration and large enhancement of electrical performances in Cu/Sb co-doped $Bi_4Ti_3O_{12}$ high temperature piezoelectric ceramics [J]. Journal of Applied Physics, 2020, 127: 044102.

[32] PENG Zhi-hang, CHEN Qiang, CHEN Yu, XIAO Ding-quan, ZHU Jian-guo. Microstructure and electrical properties in W/Nb co-doped Aurivillius phase $Bi_4Ti_3O_{12}$ piezoelectric ceramics [J]. Materials Research Bulletin, 2014, 59: 125−130.

[33] XIN De-qiong, PENG Zhi-hang, HUANG Feng-kang, CHEN Qiang, WU Jia-gang, WANG Ya-dan, YUE Xi, XIAO Ding-quan, ZHU Jian-guo. Effect of B-site dopants Nb, Ta and W on microstructure and electrical properties of $Ca_{085}(Li, Ce)_{0075}Bi_4Ti_4O_{15}-001MnCO_3$ piezoelectric ceramics [J]. Journal of Materials Science: Materials Electronics, 2016, 27: 913−920.

[34] YAN Hai-xue, LI Cheng-en, ZHOU Jia-guang, ZHU Wei-min, HE Lian-xin, SONG Yu-xin. A-site (MCe) substitution effects on the structures and properties of $CaBi_4Ti_4O_{15}$ ceramics [J]. Japanese Journal of Applied Physics, 2000, 39: 6339−6342.

[35] MOURE C, LASCANO L, TARTAJ J, DURAN P. Electrical behaviour of $Bi_5FeTi_3O_{15}$ and its solid solutions with $CaBi_4Ti_4O_{15}$ [J]. Ceramics International, 2003, 29: 91−97.

[36] ZENG Jiang-tao, LI Yong-xiang, YANG Qun-bao, YIN Qing-rui. Ferroelectric and piezoelectric properties of vanadium-doped $CaBi_4Ti_4O_{15}$ ceramics [J]. Materials Science Engineering B, 2005, 117: 241−245.

[37] XIAO Ping, GUO Yong-quan, TIAN Mi-jie, ZHENG Qiao-ji, JIANG Na, WU Xiao-chun, XIA Zhi-guo, LIN Dun-min. Improved ferroelectric/piezoelectric properties and bright green/UC red emission in (Li,Ho)-doped $CaBi_4Ti_4O_{15}$ multifunctional ceramics with excellent temperature stability and superior water-resistance performance [J]. Dalton Trans, 2015, 44: 17366−17380.

[38] CAI Kai, HUANG Cheng-cheng, GUO Dong. Significantly enhanced piezoelectricity in low-temperature sintered Aurivillius-type ceramics with ultrahigh Curie temperature of 800 °C [J]. Journal of Physics D: Applied Physics, 2017, 50: 155302.

[39] SHEN Zong-yang, LUO Wen-qin, TANG Yan-xue, ZHANG Shu-jun, LI Yue-ming. Microstructure and electrical properties of Nb and Mn co-doped $CaBi_4Ti_4O_{15}$ high temperature piezoceramics obtained by two-step sintering [J]. Ceramics International, 2016, 42: 7868−7872.

[40] HUSSAIN A, QAISER M A, ZHANG Ji, ZHANG Shan-tao, WANG Yi-ping, YANG Ying, LIU Zhi-guo, YUAN Guo-liang. High-temperature piezoelectric properties of 0−3 type $CaBi_4Ti_4O_{15}$: $x$wt%$BiFeO_3$ composites [J]. Journal of the American Ceramic Society, 2017, 100: 3522−3529.

[41] YAN Hai-xue, LI Cheng-en, ZHOU Jia-guang, ZHU Wei-min, HE Lian-xin, SONG Yu-xin, YU You-hua. Effects of A-Site (NaCe) substitution with Na-deficiency on structures and properties of $CaBi_4Ti_4O_{15}$-based high-curie-temperature ceramics [J]. Japanese Journal of Applied Physics, 2001, 40: 6501−6505.

[42] WANG Zhong-ming, CHEN Xiao-feng, CHAO Xiao-lian, WANG Juan-juan, LIANG Peng-fei, YANG Zu-pei. Low temperature sintering and dielectric properties of $(Ba_{085}Ca_{015})(Ti_{09}Zr_{01})O_{3-x}Cu^{2+}$, ceramics obtained by the sol−gel technique [J]. Ceramics International, 2016, 42: 18037−18044.

[43] LONG Chang-bai, FAN Hui-qing, LI Meng-meng, DONG Guang-zhi, LI Qiang. Crystal structure and enhanced electromechanical properties of Aurivillius ferroelectric ceramics, $Bi_4Ti_{3-x}(Mg_{1/3}Nb_{2/3})_xO_{12}$ [J]. Scripta Materialia, 2014, 75(3): 70−73.

[44] LONG Chang-bai, REN Wei, ZHENG Kun, FAN Hui-qing. Ultrahigh-temperature piezoelectric polycrystalline ceramics: Dramatically enhanced ferroelectricity, piezoelectricity and electrical resistivity in $Ca_{1-3x}Bi_{2+3x}Nb_{2-x}Mn_xO_9$ [J]. Materials Research Letters, 2020, 8(4):165−172.

[45] LONG Chang-bai, WANG Bo, REN Wei, ZHENG Kun, FAN Hui-qing, WANG Da-wei, LIU Lai-jun. Significantly enhanced electrical properties in $CaBi_2Nb_2O_9$-based high-temperature piezoelectric ceramics [J]. Applied Physics Letters, 2020, 117: 032902.

[46] CHO S Y, CHOI G P, BU S D. Comparison between the electrical properties of bismuth layer-structured and intergrowth bismuth layer-structured ferroelectric ceramics [J]. Journal Korean Physical Society, 2017, 70: 934−938.

[47] NIE Rui, CHEN Qiang, LIU Hong, XING Jie, ZHU Jian-guo, XIAO Ding-quan. MnO_2-doped $(Ca_{04},Sr_{06})Bi_4Ti_4O_{15}$ high-temperature piezoelectric ceramics with improved thermal stability [J]. Journal of Materials Science, 2016, 51: 5104−5112.

[48] XIE Juan, ZHONG Jian-qiang, WU Chao, SHI Yulin, WANG Dan, LIU Gang, LIANG Da-yun, WANG Bo, ZHU Jian-guo, CHEN Qiang. Enhanced electrical properties related to structural distortion of $CaBi_2Nb_2O_9$-based piezoelectric ceramics [J]. Journal of the American Ceramic Society, 2019,102: 1287−1295.

具有优异压电活性的 Sb−Mn 共改性的 $CaBi_4Ti_4O_{15}$ 压电陶瓷

刘 洋[1]，余 洋[1]，尹晨懿[1]，郑 梁[1]，郑 鹏[1]，白王峰[2]，李丽丽[1]，汶 飞[1]，张 阳[1]

1. 杭州电子科技大学 电子科学与技术系 纳米电子学与纳电子器件实验室，杭州 310018；
2. 杭州电子科技大学 材料与环境工程学院，杭州 310018

摘 要：采用常规烧结方法合成不同 Sb−Mn 共掺杂量的 $CaBi_4Ti_4O_{15}$ (CBT)基 Aurivillius 高温压电陶瓷。从晶体结构、显微组织和压电性能等方面研究掺杂量(x)对陶瓷性能的影响。研究发现，适当的 Sb−Mn 掺杂量可以有效地优化 CBT 陶瓷的晶格结构，降低氧空位浓度，从而提高其电学性能。在 x=0.05 组分时获得优化的电性能，792 °C 的高居里温度、25 pC/N 的压电系数(d_{33})。另外，这种陶瓷表现出良好的热稳定性，在 600 °C 退火 2 h 后 d_{33} 仍保持初始值的 88%。此外，在 400 °C 时陶瓷还显示出高电阻率(ρ=1.35×10^8 Ω·cm)和小的介电损耗(tan δ=1.7%)。由于这些优异的压电性能，Sb−Mn 共掺杂的 CBT 陶瓷有可能成为高温压电应用的潜在候选材料。

关键词：钛酸铋钙；压电陶瓷；压电活性；电阻率；热稳定性

(Edited by Xiang-qun LI)